journal of the mechanical behavior of biomedical materials 112 (2020) 104013

Contents lists available at ScienceDirect

Journal of the Mechanical Behavior of Biomedical Materials

journal homepage: http://www.elsevier.com/locate/jmbbm

Effects of melatonin on the passive mechanical response of arteries in chronic hypoxic newborn lambs

Eugenio Rivera [a], Claudio García-Herrera [a,*], Alejandro González-Candia [d,e], Diego J. Celentano [c], Emilio A. Herrera [b,d]

[a] Departamento de Ingeniería Mecánica, Universidad de Santiago de Chile, Av. Bernardo O'Higgins, 3363, Santiago de Chile, Chile
[b] Laboratorio de Función y Reactividad Vascular, Programa de Fisiopatología, ICBM, Universidad de Chile, Av. Salvador 486, Santiago de Chile, Chile
[c] Departamento de Ingeniería Mecánica y Metalúrgica, Pontificia Universidad Católica de Chile, Av. Vicuña Mackenna 4860, Santiago de Chile, Chile
[d] International Center for Andean Studies (INCAS), Universidad de Chile, Baquedano S/n, Putre, Chile
[e] Institute of Health Sciences, University of O'Higgins, Libertador Bernardo O'Higgins 611, Rancagua, Chile

ARTICLE INFO

Keywords:
Biomechanical properties
Aorta
Main pulmonary
Neonate
Chronic hypoxia
Melatonin

ABSTRACT

Chronic hypoxia is a condition that increases the cardiovascular complications of newborns gestated and born at high altitude (HA), over 2500 m above sea level (masl). A particularly complex pathology is pulmonary arterial hypertension of the neonate (PHN), which is increased at HA due to hypobaric hypoxia. Basic and clinical research have recognized that new treatments are needed, because current ones are, in general, palliative and with low effectiveness. Therefore, recently we have proposed melatonin as a potential adjuvant treatment to improve cardiopulmonary function. However, melatonin effects on the mechanical response of the arteries and their microstructure are not known. This study assesses the effects of a neonatal treatment with daily low doses of melatonin on the passive biomechanical behavior of the aorta artery and main pulmonary artery of PHN lambs born in chronic hypobaric hypoxia (at 3600 masl). With this purpose, ex-vivo measurements were made on axial stretch, tensile and opening ring tests together with a histological analysis to explore the morphometry and microstructure of the arteries. Our results show that the passive mechanical properties of the aorta artery and main pulmonary artery of lambs do not seem to be affected by a treatment based on low melatonin doses. However, we found evidence that melatonin has microstructural effects, particularly, diminishing cell proliferation, which is an indicator of antiremodeling capacity. Therefore, the use of melatonin as an adjuvant against pathologies like PHN would present antiproliferative effect at the microstructural level, keeping the macroscopic properties of the aorta artery and main pulmonary artery.

1. Introduction

Adverse conditions during the gestational period are related to fetal risks and cardiovascular diseases after birth and in adulthood (Hanson and Gluckman, 2014). For instance, intrauterine nutrition (undernutrition or overnutrition) and hypoxia are known conditions that impact on cardiac morphometry and cardiopulmonary bed, leading to a higher disease risk (Meyrick and Reid, 1982; Dong et al., 2005, 2008; Herrera et al., 2007, 2014b; Kandadi et al., 2013; Torres et al., 2015; Astorga et al., 2018; Rood et al., 2019; Hanson, 2019; González-Candia, 2020).

In particular, exposure to chronic hypoxia due to geographic high altitude (HA, >2500 masl) is a factor that increases fetal and neonatal complications (Keyes et al., 2003; Herrera et al., 2014a, 2015; Rood et al., 2019), negatively affecting the respiratory, cardiovascular and endocrine systems. Furthermore, chronic hypoxia impairs metabolism and growth, and may cause fetal abnormalities or death (Rood et al., 2019). One of the noteworthy respiratory diseases that augments due to HA hypoxia is the pulmonary hypertension of the newborn (PHN), a syndrome characterized by maintaining a high pulmonary vascular resistance (PVR) and pulmonary arterial pressure (PAP) after birth (; Hernández-Díaz, 2007; Rood et al., 2019). In addition, under this conditions, there are important structural and functional alterations of the blood vessels, such as endothelial dysfunction and vascular remodeling (Herrera et al., 2007; Gao and Raj, 2011; Papamatheakis et al., 2013; Herrera et al., 2015). In particular, vascular remodeling, associated with PHN, is a process that involves increased thickening of tunica media and

* Corresponding author.
E-mail address: claudio.garcia@usach.cl (C. García-Herrera).

https://doi.org/10.1016/j.jmbbm.2020.104013
Received 26 January 2020; Received in revised form 15 April 2020; Accepted 26 July 2020
Available online 8 August 2020

stiffening of arterial walls (Papamatheakis et al., 2013). This process is also associated with an important luminal area reduction in small pulmonary arteries (Stenmark et al., 1987; Herrera et al., 2008; Gao and Raj, 2011). Furthermore, similar changes have been found in the large pulmonary arteries of newborns exposed to chronic hypoxia (Meyrick and Reid, 1982; Astorga et al., 2018).

The current therapeutic indications for PHN include inhaled nitric oxide (iNO), surfactants, Ca2+ channel blockers, oxygen supplementation and external vital support. However, the effectiveness of the treatments is limited, because when they are suspended the problem reappears in almost 50% of the newborns, with a high morbidity and mortality (Hernández-Díaz, 2007; Gasque, 2009). Therefore, new treatments are needed to improve survival and posterior life quality of newborns suffering from PHN (Dan-Chen, 2013). Consequently, novel therapeutic approaches have been proposed with new vasoactive and antioxidant agents (Jain and McNamara, 2015; Pedersen et al., 2018). Such is the case of melatonin, a neurohormone that has important cardiovascular beneficial properties (Sun, 2016; Zhou et al., 2018). Melatonin is an antioxidant, acting as a direct scavenger of reactive oxygen species (ROS), upregulating antioxidant enzymes expression and activity, and negatively modulating pro-oxidant activity (Aversa et al., 2012; Torres et al., 2015; González-Candia, 2020), Furthermore, it has been shown to be a antihypertensive, both at systemic (Baker and Kimpinski, 2018) and pulmonary circulations (Aversa et al., 2012; Torres et al., 2015; González-Candia, 2020).

Finally, melatonin has antiremodeling effect, since it increases vascular density and luminal surface area of the pulmonary arteries, and decreases cellular density and remodeling markers (Torres et al., 2015; Astorga et al., 2018). All of these properties, improve the pulmonary vascular function and structure in the neonatal period in model animals suffering PHN (Torres et al., 2015; Astorga et al., 2018; González-Candia, 2020).

However, few is known about the biomechanical effects of melatonin on the main systemic and pulmonary arteries in the neonatal period. Knowing and evaluating the biomechanical properties of the main arteries of the circulatory system is essential and of extreme interest in the analysis of clinical cases associated with cardiovascular and cardiopulmonary problems, since they are useful for the development of a proper diagnostic (Laurent et al., 2006; García-Herrera, 2008; Dodson et al., 2013), and accurate prognosis after interventions (Claes, 2010; Akentjew et al., 2019).

Based on the above, the objective of the present research is to evaluate the effects of a treatment with low doses of melatonin on the passive mechanical properties of the aorta and main pulmonary arteries of lambs conceived and born under chronic hypoxia at high altitude (3600 masl) suffering from PHN. To that end, we describe the materials and methods used for the biomechanical (axial stretch, tensile and ring opening tests) and microstructural tests (histomorphometry), from which a number of parameters are derived that allow comparing the responses of the material.

2. Material and methods

2.1. Material

Eleven newborn lambs (*Ovis aries*) were conceived, born, and studied at high altitude (International Center for Andean Studies, INCAS Research Station), Putre, 3600 masl, GPS coordinates 18°11′47.9″S 69°33′16.5″W). In this environment, the animals develop PHN due to their conception, development and birth under chronic hypobaric hypoxia (Herrera et al., 2007, 2015; Torres et al., 2015; González-Candia, 2020).

It should be noted that at present, animal models are still important to understand the effects of exposure to hypoxia, since conditions can vary from mild to extreme when analyzing cases of interest (Rood et al., 2019). In particular, the models of fetal and newborns sheep raised at high altitude are similar to human newborns affected by hypobaric hypoxia (Herrera et al., 2007; Rood et al., 2019), showing similar cardiovascular and respiratory development and body weight (Rood et al., 2019).

Table 1
General information of the individuals tested: the control group (CN, $n = 6$) and melatonin group (MN, $n = 5$). Average values were expressed as Mean ± SEM.

Lamb	Weight [kg]	Age [days]	Lamb	Weight [kg]	Age [days]
CN1	8.1	31	MN1	7.7	32
CN2	9.1	33	MN2	3.9	32
CN3	5.2	33	MN3	9.2	33
CN4	9.1	29	MN4	10.9	32
CN5	7.4	30	MN5	9.1	29
CN6	10.2	30	–	–	–
Mean	**8.2±0.7**	**31±1**	**Mean**	**8.2±1.2**	**32±1**

The lambs were separated randomly into two groups:

Control (CN): Six lambs were administered the vehicle orally (CN, $n = 6$, 1.4% ethanol 0.5 mL kg^{-1} per day).

Melatonin (MN): Five lambs were treated with oral melatonin (MN, $n = 5$, melatonin 1 mg kg^{-1} in ethanol 1.4%, 0.5 mL kg^{-1} per day).

Melatonin or vehicle administration was performed during 21 days from the third day of life, at dusk (20:00 h) to follow the circadian rhythm of melatonin nocturnal endogenous release.

Previous studies using sheep neonates as a model of PHN (Torres et al., 2015; González-Candia, 2016; González-Candia, 2020) have demostrated that the administration of a dose of 1 mgKgg^{-1} increases the plasma levels of melatonin without affecting the daytime concentrations of this hormone, maintaining the circadian rhythm of plasma concentration. Moreover, one dose is capable of increasing melatonin levels about nine times after 1 h (Torres et al., 2015; González-Candia, 2020).

All the arterial samples were obtained from lambs aged between 29 and 33 days old, as shown in the general data of Table 1.

Each aorta was divided according to two regions: thoracic aorta (TA) and abdominal aorta (AA). Thereafter, aorta artery and main pulmonary artery (MPA) were preserved in a saline solution (Krebs) cooled to 4°C until experiments. The biomechanical tests were performed not more than 24 h after extraction.

Animal care, maintenance and procedures were approved by the Bioethics Committee of the Faculty of Medicine of the Universidad de Chile (CBA # 0761 FMUCH) and were carried out according to the International Regulations for the Care and Use of Laboratory Animals published by the National Institutes of Health of The Unites States (Publication NIH No. 85–23, revised in 1996).

2.2. Biomechanical tests

2.2.1. Axial stretch tests

It is known that in the physiological state many arteries (e.g. the artery aorta) are under an axial stretch. This is evident when cutting an artery and observing a longitudinal shortening. To quantify this change in length, a measurement process is performed, where the initial or physiological lengths (before cutting) are recorded and compared with the measurements after the artery was extracted. The measurement procedure followed in this work consisted of dividing the length of the thoracic aorta (TA) and abdominal aorta (AA) into five equal segments according to their length, before excision. Subsequently, the observed shortening was recorded in photographs. The procedure allows to calculate the physiological length of the artery, l_f and similarly the longitudinal measurements of the artery are obtained once it is extracted, that is, the length, L. The axial stretch is computed as:

$$\lambda_z = \frac{l_f}{L}\,. \tag{1}$$

Table 2
Average values of the dimensions in the rectangular samples for both CN and MN groups used in the uniaxial tensile test. Values were expressed as Mean ± SEM. Significant differences ($P \leq 0.05$): * vs. CN.

Artery (Circ. Direction)	Thickness [*mm*]	Length [*mm*]	Width [*mm*]
TA CN	1.74±0.03	6.74±0.09	5.34±0.26
TA MN	1.95±0.09	7.03±.0.17	6.26±0.50
AA CN	0.82±0.02	6.89±0.45	5.99±0.45
AA MN	0.77±0.06	7.17±0.15	5.17±0.44
MPA CN	1.87±0.03	6.49±0.11	4.59±0.18
MPA MN	1.96±0.04	6.76±0.07	5.76±0.29
Artery (Long. Direction)	Thickness [*mm*]	Length [*mm*]	Width [*mm*]
TA CN	1.78±0.05	6.86±0.14	6.38±0.22
TA MN	1.93±0.09	6.91±0.21	6.45±0.23
AA CN	0.81±0.04	7.02±0.15	6.88±0.68
AA MN	0.78±0.07	6.04±0.13	5.85±0.40

The quantification of the axial stretch is intended to evaluate the changes produced by the administration of melatonin, and derive some biomechanical parameters of interest (distensibility and incremental module). In addition, this measure can be used in future research, to perform more realistic computational simulations of the mechanical response of the aorta artery according to the zone of interest.

It should be noted that in the case of the MPA this measure was not evaluated, due to the physiological limitations of its size and location, and in this work it is assumed free of axial stretch.

2.2.2. Tensile test

The tensile test is aimed at determining the stress-stretch relation under uniform deformation. Although the uniaxial stress experiments are insufficient to characterize completely the constitutive three-dimensional stress-stretch relations of the biological materials, these tests can provide useful descriptive information on the mechanical behavior (Macrae, 2016). In the present work it is used mainly to obtain biomechanical responses that allow comparing the studied groups. The experimental protocol was adjusted to physiological conditions as established by García-Herrera, (2008), with samples immersed in calcium-free saline solution (Krebs), at 39^oC.

The samples subjected to tension were obtained from the arteries by cutting rectangular strips in the circumferential and longitudinal directions. The average values of the geometry of the samples are presented in Table 2. The samples were mounted and stretched to rupture at a constant speed of 1.5 mm/min in an Instron 3342 machine equipped with a 10 N load cell with a precision ±0.001N.

In this test, the Cauchy's axial stress is calculated as $\sigma = \frac{F}{A}$, where F is the axial load and A is the instantaneous cross sectional area. The axial stretching is calculated as $\lambda = \frac{L}{L_0}$, where L and L_0 are the instantaneous and initial measurements of the sample, respectively. The instantaneous cross-sectional area A is evaluated through the incompressibility condition that leads to $A = \frac{A_0}{\lambda}$, where A_0 is the sample's initial cross sectional area (García-Herrera et al., 2016).

The results of the test were used to determine some biomechanical parameters that allow comparing the tensile mechanical behavior, which are, for the physiological function range, the distensibility and the

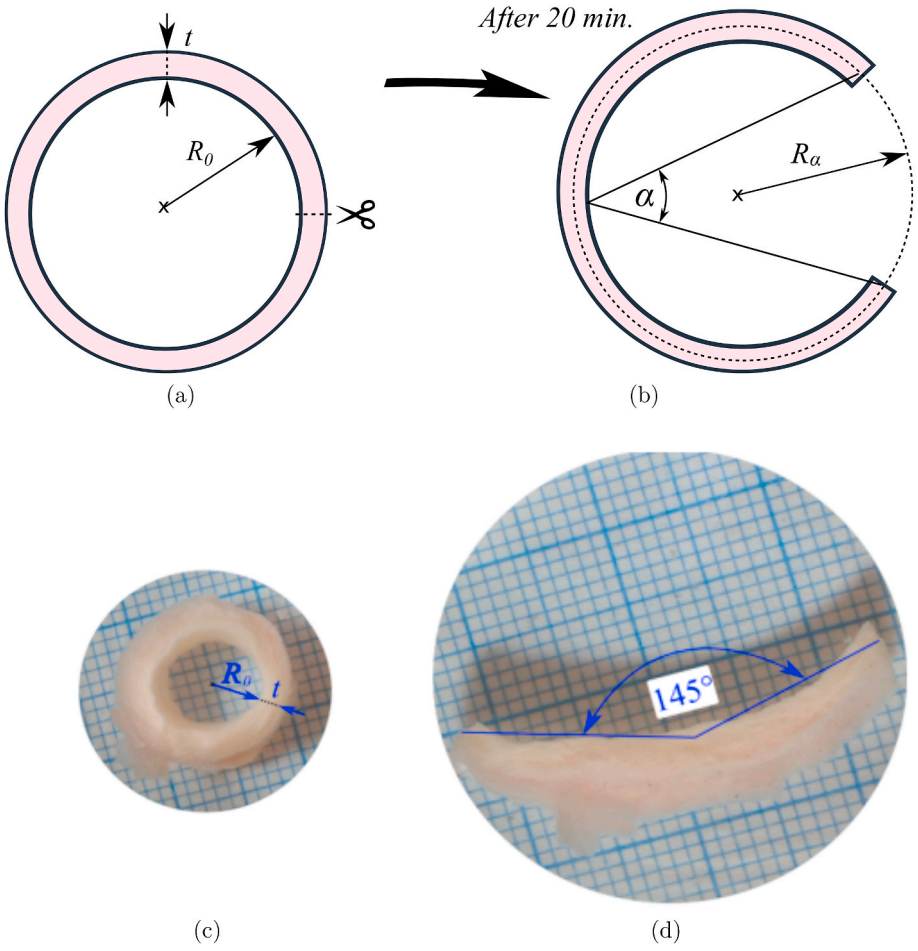

Fig. 1. Representation of the opening the rings process. (a) Initial and (b) Open configurations. R and t respectively denote the radius and thickness, α represents the opening angle. Representative samples of opening rings of thoracic artery. (c) Initial and (d) Open configurations.

incremental module, where the thin-walled tube approximation is assumed as in the work by (García-Herrera, 2012). In addition, to evaluate the global behavior the initial and final slopes, the elbow point, and rupture values of the stress-stretch curves were determined (Cañas et al., 2017).

The distensibility proposed by Laurent et al., (2006) (Laurent et al., 2006), is given by:

$$DC = \frac{D_s^2 - D_d^2}{D_s^2\,(P_s - P_d)} \tag{2}$$

where D_s and P_s are the diameter and the systolic pressure, respectively, while D_d and P_d are the diameter and the diastolic pressure, respectively (systolic pressure $\approx$ 120 *mmHg* and diastolic pressure $\approx$ 60 *mmHg*) (Peers et al., 2002).

For the main pulmonary artery we consider that the physiological pressures are between 14 and 35 *mmHg*, values close to those reported by (Eisele, 1986; Drude et al., 2000; Thelitz et al., 2004; Herrera et al., 2007).

The formula to obtain the incremental module which represents the secant to the $\sigma - \lambda$ curve in the physiological pressure values (systolic and diastolic) is given by expression 3 (Laurent et al., 2006):

$$E_{inc} = \frac{3D_s^2(P_s - P_d)}{D_s^2 - D_d^2}\,\frac{4t + D_s}{4t} = \frac{3}{DC}\,\frac{4t + D_s}{4t} \tag{3}$$

where t is average initial unloaded arterial wall thickness.

The initial and final slopes of the stress-stretch curves were determined by fitting a linear regression, selecting the points of the curve until a variation smaller than or equal to 5%. The point that defines the elbow of the curves was calculated directly from the final coordinate of the linear zone E_1 and the initial coordinate of the final zone E_2 according to Cañas et al. (2017).

2.2.3. Ring opening tests

The estimation of the ring opening in the blood vessels is an aspect that must be evaluated to achieve a more robust characterization of the material response (García-Herrera et al., 2016). In this work the ring opening test (Vaishnav and Vossoughi, 1983; Liu and Fung, 1988; Okamoto et al., 2002; Holzapfel et al., 2007) was used to evaluate the changes due to the administration of melatonin. The test consists basically in cutting in the radial direction a ring-shaped arterial piece, which due to internal stresses is opened until stabilization is achieved. The angle formed by the cut ends defines the opening angle, α, as can be seen in Fig. 1a and b.

Samples of 4 mm height were used. The procedure consisted in measuring the sizes of the ring-shaped samples, which were then immersed in Krebs during 10 min at a temperature of 39 ± 1°C (physiological range for lambs). The rings were then cut radially, and after 20 min in the saline solution the resultant opening angles were measured. The sizes of the samples and the opening angles were obtained by image processing using the imageJ software (Schneider, 2012).

2.3. Histomorphometry

The composition and structure of the tissues were studied through histological and morphometric analyses previously described by Carson and Hladik (2009) (Carson and Hladik, 2009; Astorga et al., 2018).

Ring-shaped aorta artery pieces from the thoracic and abdominal zones were extracted, and they were immersed and fixed in 4% paraformaldehyde during 24 h at 4°C. The samples were embedded in paraffin and cut in 5 μm thickness cross sections on a Leitz rotary microtome. The sections were mounted on microscope slides and stained with the Hematoxilin-Eosin (HE) and Elastic van Gieson (EVG) stains. The observation and capture of the micrographs were made under an Olympus BX41 microscope and a Jenoptik digital camera model ProgRes®C3 (Jena, Germany), for 4X, 10X, and 40X magnifications

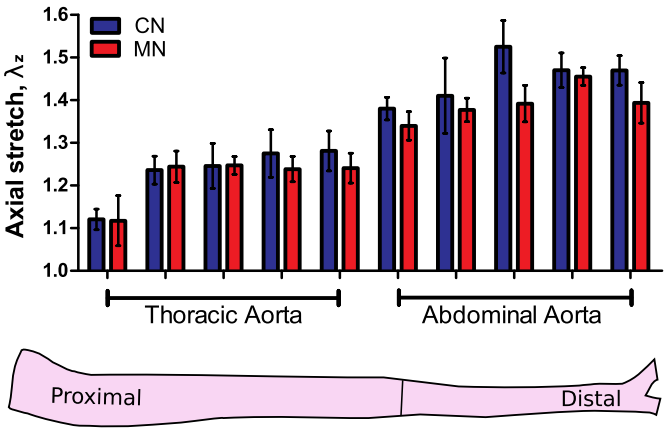

Fig. 2. Axial stretch. Groups are control (CN, $n = 6$) and melatonin (MN, $n = 5$) lambs. Values are means ± SEM. Significant differences ($P \leq 0.05$): * vs. CN.

(Astorga et al., 2018).

Micrographs were taken to (1) observe the general state of the blood vessels; (2) quantify the density of elastin and collagen cell components (n° of component pixels/total pixels) in the tunica media of each artery; (3) determine cellular density per area (n° of smooth muscle nuclei/ ($50 \times 50\ \mu m^2$)) in the tunica media of each artery; and (4) perform morphological measurements of the arterial wall, including measurements of internal and external diameters, wall thicknesses, and wall layers thicknesses. These processes were developed with computational support using ImageJ 1.48v (Schneider, 2012) and GIMP 2.10.2 (GIMP-team, 2014) softwares.

2.4. Statistic analysis

All the data were expressed as the *means ± standard error of the mean* (SEM), which is the ratio between the standard deviation and the square root of the number of specimens.

All the results were compared statistically by means of the non-parametric Mann-Whitney test for independent random samples. Significant differences were accepted when $P \leq 0.05$ (Prism 5.0; GraphPad).

3. Results and discussion

3.1. Axial stretch

Fig. 2 presents the graphs of the average axial stretch along the aorta artery for the control (CN) and melatonin (MN) groups, respectively. It should be remembered that, each zone (TA and AA) was divided into five segments as explained in the 2.2.1 section. The results obtained show a variable response along the aorta artery. At the proximal end, the lowest axial stretch value is presented ($\approx$ 1.118, for both CN and MN), followed by an increase to mean values for the thoracic zone (CN: 1.260 ± 0.011; MN: 1.242±0.002). And then, a new increase is evident when crossing the transition zone (thoracic-abdominal), the average values obtained in the abdominal zone were similar (CN: 1.451 ± 0.025; MN: 1.392 ± 0.018). The comparison in the axial stretch responses between the CN and MN groups does not show significant statistical changes, the greatest variation observed corresponds to the eighth section, where the MN group presents a decrease equivalent to 8.7% with respect to the CN group.

Axial stretch analyzes have been performed on the human thoracic and abdominal aorta. The mean value for the thoracic zone is $\lambda_z = 1.20$ (Holzapfel et al., 2007; García-Herrera, 2012), and for the abdominal section samples is $\lambda_z = 1.37$, with a tendency to decrease with age (Horny, 2013). The indicated data is widely used to analyze the mechanical behavior of the aortic artery in sheep and human models

Table 3
Average values of parameters obtained from the stress-stretch curve for the aorta artery and main pulmonary artery: initial slope E_1 and final slope E_2, coordinates of the elbow (λ_c, σ_c) and coordinates of the rupture (λ_r, σ_r). Values were expressed as Mean ± SEM. Significant differences ($P \leq 0.05$): * vs. CN.

TA	Thoracic aorta artery					
	$E_1\,[kPa]$	$E_2\,[kPa]$	$\lambda_c\,\left[\frac{mm}{mm}\right]$	$\sigma_c\,[kPa]$	$\lambda_r\,\left[\frac{mm}{mm}\right]$	$\sigma_r\,[kPa]$
Long. CN	37.13±9.30	426.0±124.5	1.40±0.05	27.23±6.94	2.14±0.13	291.6±92.6
Long. MN	33.21±5.19	353.7±99.5	1.40±0.09	23.54±6.05	2.10±0.10	235.4±37.2
Circ. CN	62.27±7.90	653.1±120.7	1.64±0.05	77.04±11.94	2.49±0.14	615.9±133.6
Circ. MN	52.46±9.06	525.7±45.6	1.55±0.05	59.70±4.77	2.39±0.12	452.0±33.7
AA	Abdominal aorta artery					
	$E_1\,[kPa]$	$E_2\,[kPa]$	$\lambda_c\,\left[\frac{mm}{mm}\right]$	$\sigma_c\,[kPa]$	$\lambda_r\,\left[\frac{mm}{mm}\right]$	$\sigma_r\,[kPa]$
Long. CN	91.6±16.05	2295±432	1.60±0.09	152.6±29.9	2.57±0.19	1784±310
Long. MN	95.6±19.73	2284±905	1.54±0.07	106.4±28.2	2.44±0.13	1632±665
Circ. CN	163.6±36.6	2651±409	1.50±0.08	153.9±33.3	2.21±0.15	1543±268
Circ. MN	183.9±40.0	2607±331	1.44±0.05	167.6±34.4	2.16±0.11	1599±381
MPA	Main pulmonary artery					
	$E_1\,[kPa]$	$E_2\,[kPa]$	$\lambda_c\,\left[\frac{mm}{mm}\right]$	$\sigma_c\,[kPa]$	$\lambda_r\,\left[\frac{mm}{mm}\right]$	$\sigma_r\,[kPa]$
Circ. CN	22.7±4.0	463.2±68.8	1.64±0.04	38.17±7.07	2.79±0.14	423.5±72.3
Circ. MN	19.2±2.8	371.1±13.1	1.70±0.11	36.24±7.55	3.16±0.32	482.2±102.7

Table 4
Distensibility, *DC*, and incremental modulus of elasticity, E_{inc}, obtained in the tensile test. Values were expressed as Mean ± SEM. Significant differences ($P \leq 0.05$): * vs. CN.

Artery	Stretching	$DC\,[mmHg^{-1}] \times 10^{-3}$	$E_{inc}\,[MPa]$
TA CN	$\lambda_z = 1.23$	6.05±0.55	0.242±0.023
TA MN	$\lambda_z = 1.22$	5.70±0.37	0.243±0.017
AA CN	$\lambda_z = 1.45$	3.88±0.46	0.538±0.044
AA MN	$\lambda_z = 1.39$	3.56±0.52	0.591±0.092
MPA CN	$\lambda_z = 1.00$	14.5±1.3	0.096±0.010
MPA MN	$\lambda_z = 1.00$	15.9±1.7	0.083±0.005

(García-Herrera, 2012; Horny, 2014; Dodson et al., 2014). Furthermore, our results (see Fig. 2 or Table 4) are close to those reported in such references.

3.2. Tensile test

Fig. 3a and b show the graphs of the average stress-stretch curves of the thoracic aorta for the control (CN) and melatonin (MN) groups, respectively. Similarly, Fig. 3c and d present the graphs of the average stress-stretch curves of the abdominal aorta. Each figure contains the experimental data for the circumferential and longitudinal directions. An estimation is also made of the rupture point, which we define by the pair of coordinates: mean rupture stretch (λ_r) and mean rupture stress (σ_r), shown in Table 3. It is seen that all the curves present a typical hyperelastic behavior, that is, a first linear stage followed by a transition stage, and finally a linear (stiffening stage). Analogously, Fig. 3e shows the graphs of the average stress-stretch curves of the main pulmonary artery for the control (CN) and melatonin (MN) groups for the circumferential direction. From the stress-stretch curve a set of parameters (initial and final slopes together with elbow coordinates) were derived which allow comparing the mechanical responses of the arteries (Table 3). The values in general do not present significant changes between the MN group and the CN group, but a large part of the average values of the parameters of the MN group present a decrease of the mechanical properties compared to the CN group, particularly in the thoracic aorta the differences exceed 10% difference compared to the CN group. In the abdominal aorta the results show a large similarity between groups. The distensibility and incremental module measurements presented in Table 4 show similar biomechanical responses in the physiological pressure range ($P_d = 60\ mmHg$, $P_s = 120\ mmHg$) for the aorta artery and main pulmonary artery ($P_d = 14\ mmHg$, $P_s = 35\ mmHg$). Values that cover satisfactory the range of pressure obtain in this work SP (CN: 33.8 ± 2.7 mmHg; MN: 28.0 ± 0.3 mmHg) and DP (CN: 15.0 ± 1.3 mmHg; MN: 16.2 ± 0.9 mmHg).

On the other hand, the mechanical responses to uniaxial tensile in the thoracic artery aorta of the CN and MN groups (see Fig. 3a and b) shows that the curves in the circumferential and longitudinal directions are similar, which could wrongly mean a response close to the isotropic over the whole stretching range. However, these results correspond to an approximation of the global response of the blood vessels, and it should not be assumed directly that the behavior is isotropic (García-Herrera et al., 2016), because the arterial mechanical response presents anisotropy due to the presence of collagen fibers, and furthermore, the arterial wall is composed of three layers (intima, media, and adventitia) which differ in their mechanical behavior (Holzapfel, 2006). The results presented here must be contrasted with biaxial biomechanical tests with the purpose of evaluating if the exposure to chronic hypoxia due to high altitude affects the mechanical behavior from anisotropic to isotropic, as has been shown with other pathologies, such as, for example, Marfan's disease (García-Herrera, 2008; García-Herrera et al., 2016). The mechanical responses to uniaxial tension in the abdominal aorta artery presents a more marked anisotropic biomechanical response, as shown in Fig. 3c and d.

The mechanical responses to uniaxial tension in the main pulmonary artery of the CN and MN groups is presented in Fig. 3e, where it is shown that the curves in the circumferential direction are similar.

Additionally, we present some comparisons with values obtained in the literature. In the work by Dodson et al. (2014), two groups, one control and one with intrauterine growth restricted fetal sheep, where thickness values for aorta were compared. For the control group, they obtained thoracic aorta $t = 1.99\ mm$ and abdominal aorta $t = 0.67\ mm$, values close to those obtained in our work (see Table 2). In addition, larger values are reported for human arteries, e.g., $t = 2.60\ mm$ (García-Herrera et al., 2016). In the work of Wells et al. (1999), initial and final slope values (E_1 and E_2) for thoracic aorta samples of fetuses, lambs and adult sheep were reported from the pressurization test, which could be compared with our results in the circumferential direction. In the particular case of lambs, the values were $E_1 = 150\ kPa$ and $E_2 = 1400\ kPa$. These results are far from our results in thoracic sections, but similar to our abdominal aortic artery values (see Table 3). These

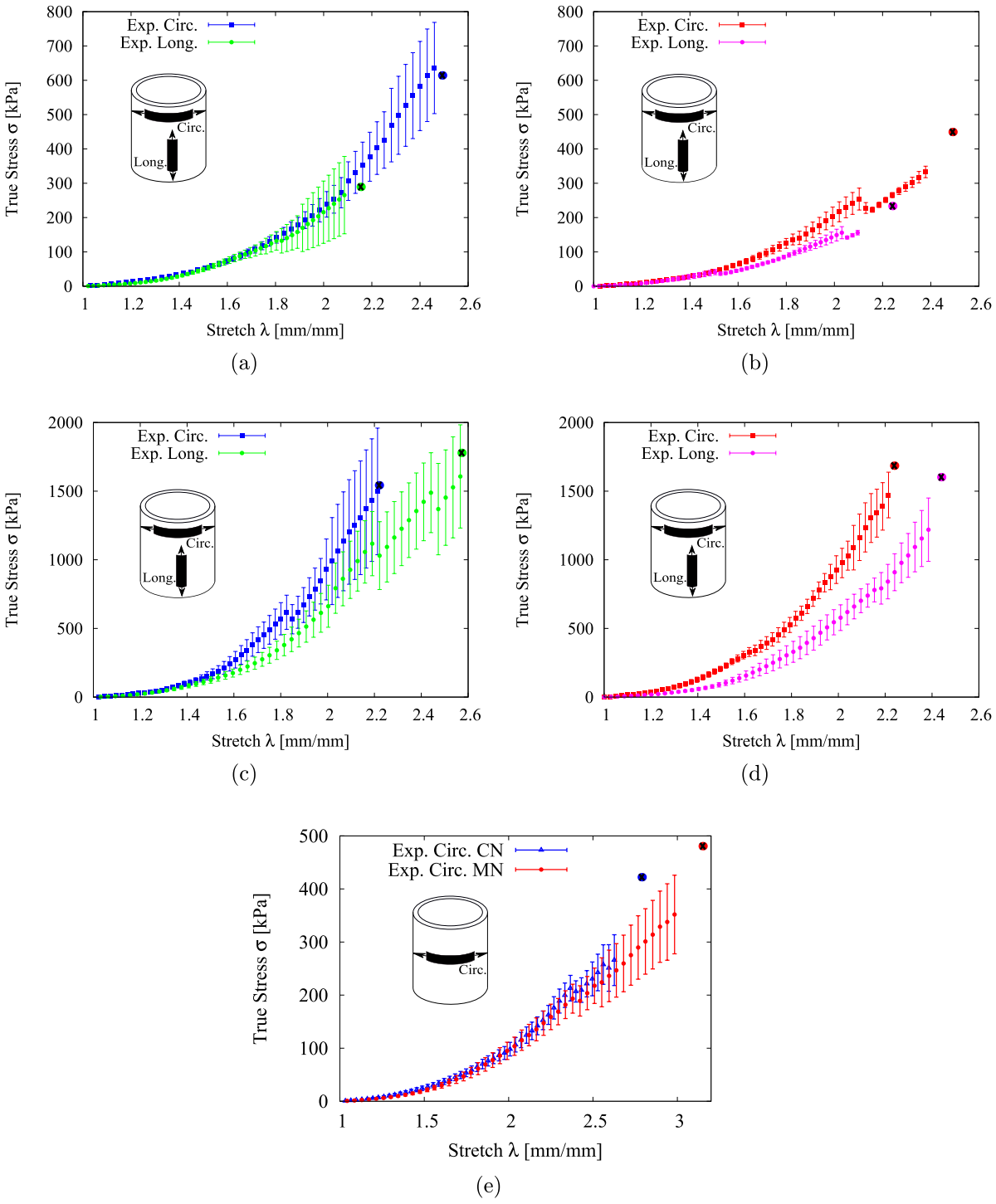

Fig. 3. Stress-stretch curves. (a) Thoracic aorta for control group (CN) lambs, (b) Thoracic aorta for melatonin group (MN) lambs, (c) Abdominal aorta for control group (CN) lambs, (d) Abdominal aorta for melatonin group (MN) lambs. and (e) Main pulmonary artery for control group (CN) and melatonin group (MN) lambs. Experimental values were expressed as Mean ± SEM. The points ⊗ represent the coordinates of the rupture points.

differences may be due to the evaluation procedure of these moduli used in both tests: local in the uniaxial test and structural in the pressurization test (Claes, 2010). The values of compliance and incremental modulus in human aortas reported by García-Herrera et al. (2016) were $4.261\times 10^{-3}\ mmHg^{-1}$ and $0.482\ MPa$, respectively. In relation to the main pulmonary artery, our thickness values are greater than those reported for pediatric pulmonary arteries ($t = 1.06\ mm$) (Cabrera et al., 2013), and less than those of an adult ovine pulmonary arteries ($t = 2.85\ mm$) reported by (Cabrera et al., 2013). On the other hand, in the aforementioned investigation, they performed equibiaxial tensile tests on MPA samples: although they cannot be directly comparable, our stress-stretch curves are similar to those of the reported sheep group.

3.3. Ring opening test

Fig. 1 shows a representative ring of a sample of a thoracic aorta artery, (c) which corresponds to a closed ring before making the radial cut, and (d) is the opened ring after the cut and the stabilization,

Table 5
Geometric data to determine the initial and final configurations in the ring opening process. Values were expressed as Mean ± SEM. Significant differences ($P \leq 0.05$): * vs. CN.

Artery	R_0 [mm]	e_0 [mm]	α [°]
TA CN	3.57±0.34	2.06±0.07	144±9
TA MN	3.26±0.15	2.14±0.07	140±16
AA CN	2.51±0.11	0.81±0.03	50.6±9.4
AA MN	2.35±0.14	0.81±0.04	48.0±9.3
MPA CN	3.80±0.52	1.81±0.14	134±8
MPA MN	3.73±0.27	1.94±0.07	153±8

configuration that allows calculating the opening angle.

Using the nomenclature defined in Fig. 1, Table 5 summarizes the geometric values for the ring opening test; these values are the internal radius R_0, the thickness e_0 and the opening angle α. The data are presented as the average ± SEM. The results obtained show similarities in the geometry of the arteries and opening angles, and the statistical evaluation does not show significant changes between the CN and MN groups. The similarity seen in the values of the opening angles agrees with what was seen in the microstructure, because specifically the opening angle is related to the presence of elastin in the arterial wall (Greenwald et al., 1997) whose amount resulted similar for the two groups CN and MN (see results in Section 3.4). On the other hand, the results show that in the thoracic zone they have greater opening angles compared to the abdominal zone, a behavior that is in agreement with those reported in (Liu and Fung, 1988; Fung, 1991) in rat aortas. Some investigations reported for the healthy human thoracic aorta (García--Herrera et al., 2016), pig and rat abdominal aortas (Kassab, 2006) have a mean opening angle of about $\alpha = 130^o$ (Kassab, 2006; García-Herrera et al., 2016), value close to that obtained for the thoracic aortic artery in our work.

3.4. Histomorphometry

Fig. 4 show representative micrographs for the cross section of aorta arteries of lambs. Fig. 4 shows the general condition of the artery which presents an ordered and well defined structure in which the elastin fibers arranged circumferentially are distinguished (Claes, 2010).

Fig. 4a corresponds to a HE stain and Fig. 4b to an EVG stain, which is a more specific trichromic stain that shows in greater detail the circumferential distribution of the elastin fibers, and the tunica intima allows the observation of the collagen (in reddish color).

With respect to the morphological measurements, it was found that the micrographs of the thoracic aorta artery showed an absence of the tunica adventitia as a result of the cleansing made of the artery before the experimental procedures (see Fig. 4a). The results of the measurements of the tunica intima and media were similar between groups. Equally, Fig. 4b shows a representative micrograph of the abdominal aorta artery, and the results of the thicknesses of the arterial wall were similar between groups (as can be seen in Table 6). The thicknesses of the main pulmonary artery layers, denoted by L1, L2, and L3 (Frid, 1994) were similar between groups, except on the thickness of zone L1 that was decreased by melatonin treatment (see Fig. 5 and Table 6). In general, the statistical evaluation does not show significant changes between the CN and MN groups. Similar results were obtained in the main pulmonary artery layers by Astorga et al. (2018), where 12-day-old lambs were analyzed under similar conditions, with a similar pharmacological treatment. The decrease in the L1 zone was attributed to the effects of melatonin in the smooth muscle cell density. We therefore speculate that L1 zone might be the most affected layer in the chronic hypoxia-induced remodeling.

The cellular density was made on HE stained samples, and the results correspond to the number of nuclei contained in a $50 \times 50\ \mu m^2$ surface. There was a decreased number of nuclei in the arteries of the melatonin

Table 6
Intima thickness, media thickness, media cellular density in the aorta artery; and L1, L2, L3 thicknesses and cellular density in de main pulmonary artery. Groups are control (CN, $n = 6$) and melatonin treated (MN, $n = 5$) lambs. Values are means ± SEM. Significant differences ($P \leq 0.05$): * vs. CN.

		Control (CN)	Melatonin (MN)
AT	Intima thickness (μm)	54.1 ± 8.2	57.5 ± 9.6
	Media thickness (μm)	1419 ± 132	1539 ± 18
	Media cellular density (cells/μm^2) × 10^{-2}	0.327 ± 0.022	0.276 ± 0.022
AA	Intima thickness (μm)	34.1 ± 5.1	29.1 ± 4.1
	Media thickness (μm)	503.2 ± 21.8	578.7 ± 25.5
	Media cellular density (cells/μm^2) × 10^{-2}	0.282 ± 0.010	0.233 ± 0,008*
MPA	L1 zone thickness (μm)	114.8 ± 4.2	96.3 ± 4.1*
	L2 zone thickness (μm)	567.2 ± 60.4	498.9 ± 29.0
	L3 zone thickness (μm)	663.7 ± 37.0	869.4 ± 110.3
	L1 zone cellular density (cells/μm^2) × 10^{-2}	0.406 ± 0,076	0.258 ± 0.046
	L2 zone cellular density (cells/μm^2) × 10^{-2}	0.232 ± 0,012	0.232 ± 0.012
	L3 zone cellular density (cells/μm^2) × 10^{-2}	0.301 ± 0,018	0.268 ± 0.019

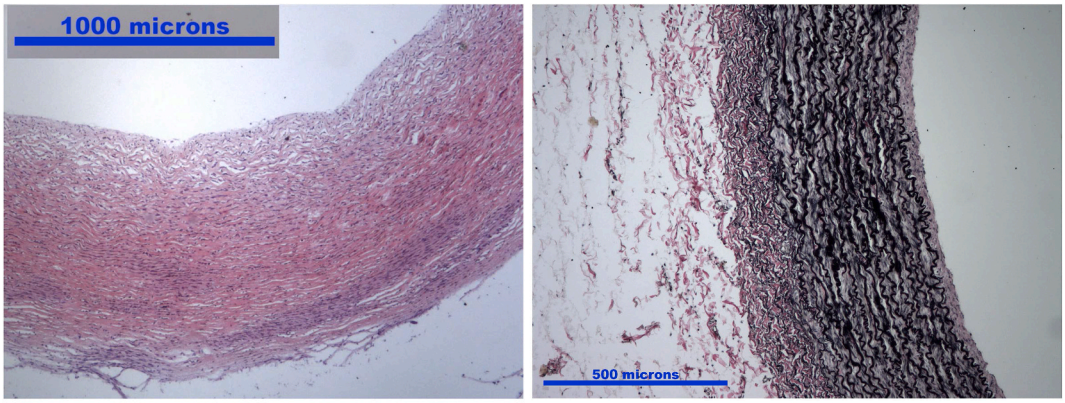

Fig. 4. Representative histological section of: (a) thoracic aorta with Hematoxylin-Eosin (HE) stain, the magnification 4X is shown. (b) abdominal aorta with Elastic Van Gieson (EVG) stain, the magnification 10X is shown.

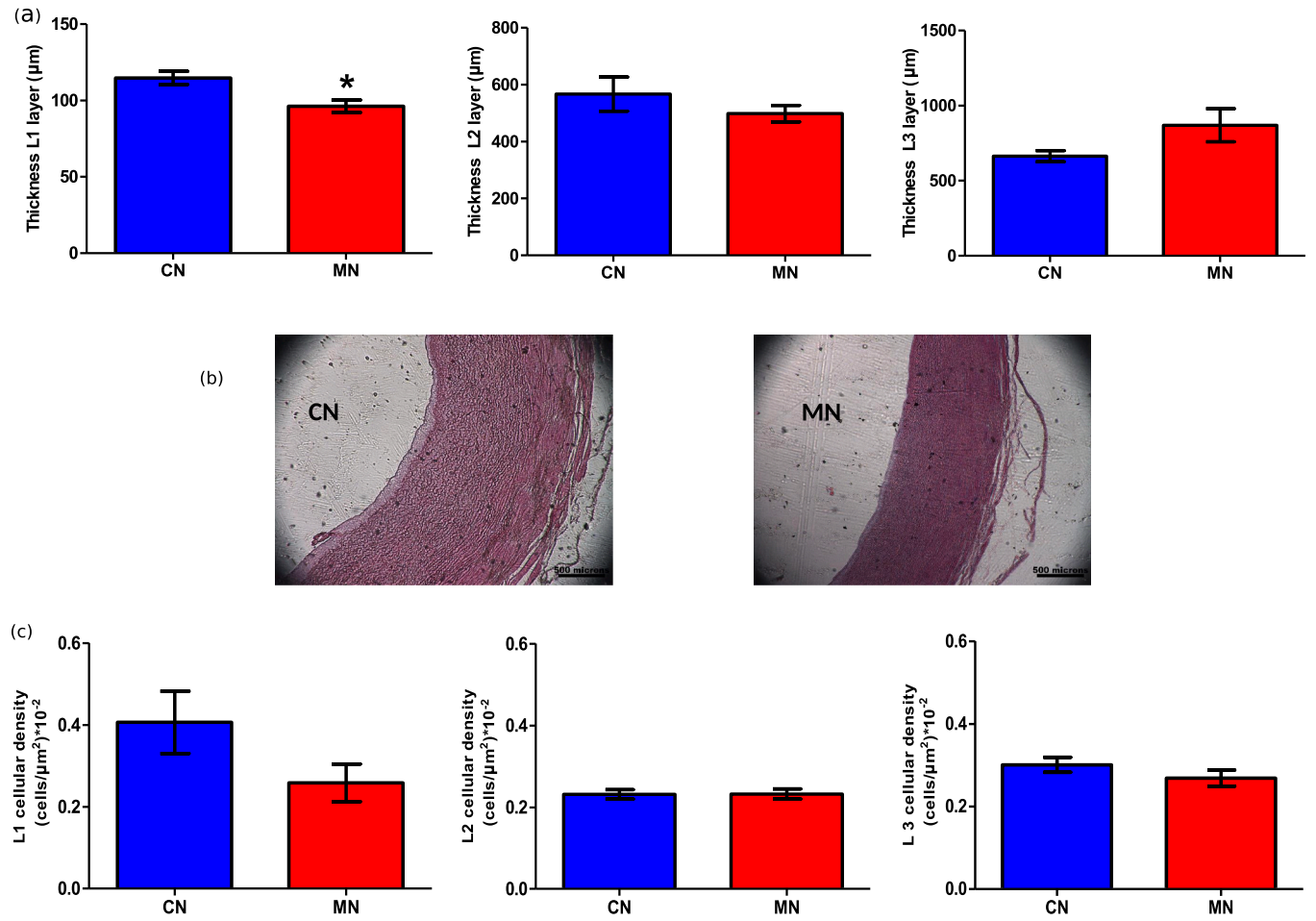

Fig. 5. Results for the main pulmonary artery. (a) Thickness of the zones (L_i, $i = 1, 2, 3$). (b) Representative histological section. (c) Cellular density in the zones (L_i, $i = 1, 2, 3$). Groups are control (CN, $n = 6$) and melatonin (MN, $n = 5$) lambs. Values are means ± SEM. Significant differences ($P \leq 0.05$): * vs. CN.

group, as shown in the graph of Fig. 6 or Table 6. The results were similar for thoracic artery and were significant for the abdominal aorta and may indicate a possible antiremodeling effect in the arterial wall caused by the administration of melatonin. However, no differences were observed in the cellular density of the zones of the main pulmonary artery, as shown in the graph of Fig. 5c. The results obtained in this work are similar to those published by Dodson et al. (2014), where it was observed that in the thoracic zone there is a higher cell density than in the abdominal zone (TA: 0.38 (cells/μm^2)$\times 10^{-2}$ and AA: 0.26 (cells/μm^2) $\times$ 10^{-2}).

Finally, the estimation of the microstructural amounts of elastin and collagen (based on the EVG stain) were similar and gave the following results for the thoracic aorta (elastin CN: 34.3±5.4%; MN: 34.5±4.6%, and collagen CN: 11.1±1.3%, MN: 11.4±1.4%). For the abdominal aorta: elastin (CN: 43.7±4.2%; MN: 40.3±0.5%) and collagen (CN: 13.8±1.8%; MN: 14.7±1.2%). In addition, the main pulmonary artery elastin was CN: 18.4±2.5%; MN: 22.3±3.6% while the collagen content was CN: 14.9±2.1%; MN: 15.2±2.4%. The statistical analysis did not show any significant differences in these variables. In the study by Dodson et al. (2014) the percentage of elastin was calculated in the aortic artery, with 27% and 33%, in the thoracic and abdominal zone, respectively. In the work of Arroyave et al. (2015), pig aortic arteries were analyzed, reporting high percentages of passive cellular content in the groups of aortic arteries, for the thoracic aortic artery where the percentage of collagen was 33.3% and that of elastin was 57.6%. For the abdominal aortic artery the percentage of collagen was 32.1% and elastin 58.0%. However, the latter samples were obtained from adult animals.

Unfortunately, one of the limitations of our study is that we do not know if the effects induced by melatonin are receptor-mediated (Astorga et al., 2018). However, a previous study has shown that in the aortic artery of rats MT1 receptors are present and were preferentially localized to the tunica adventitia, while MT2 receptors are not present (Schepelmann et al., 2011), where, in this same study, MT1 it is related to vasoconstriction and MT2 with vasodilation. Therefore, melatonin does not contribute directly to relaxation or contraction of the aorta. This could support the results obtained in the present investigation, since in general the effects of melatonin on the aortic artery were not statistically significant.

4. Conclusions

The experimental work based on the axial stretch, uniaxial tensile and ring-opening tests on samples of aorta and main pulmonary arteries have been presented. The central study case corresponded to the evaluation of the effect of the administration of melatonin on the arterial biomechanical behavior in lambs gestated and born at high altitude; affected by pulmonary arterial hypertension. The evaluation contrasted two experimental groups: the control group (CN) and the melatonin (MN) treated group.

The macroscopic analysis experimentally based on biomechanical tests, which compared the behavior of the CN and MN groups, was similar in all the biomechanical analyses (axial stretch, tensile and ring-opening tests). No evidence was found of significant changes in the general and standard comparison parameters, such as the initial and final slopes, elbow, and rupture coordinates. In addition, there were no

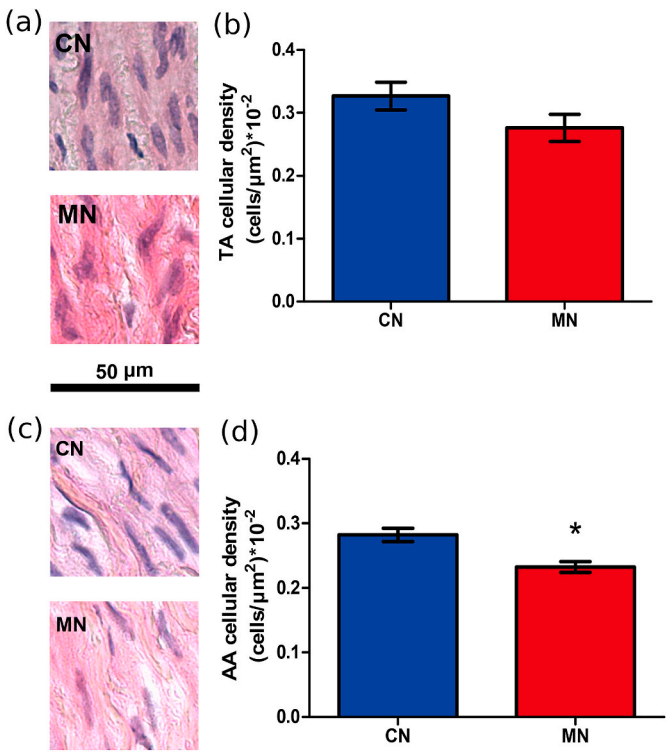

Fig. 6. Representative histological section (40X) used for the cellular density count. (a) Thoracic aorta with Hematoxylin-Eosin (HE) stain. (b) Cellular density in the media layer of the thoracic aorta. (c) Abdominal aorta with Hematoxylin-Eosin (HE) stain. (d) Cellular density in the media layer of the abdominal aorta. Groups are control (CN, $n = 6$) and melatonin (MN, $n = 5$) lambs. Values are means ± SEM. Significant differences ($P \leq 0.05$): * vs. CN.

changes in the parameters associated with the physiological functions detected, such as the distensibility and incremental modulus. Similarly, no significant changes were found in the biomechanical response due to the axial stretch and ring-opening analysis.

In addition, the microstructural analysis through the histological examination did not show any significant changes in the aortic thickness or elastin and collagen amount. However, we observed significant changes in the thickness L1 layer of the main pulmonary artery and the cell density contained in the arterial wall of the abdominal aorta. This changes that may represent an antiremodeling process as a result of the administration of melatonin in the neonatal period (Astorga et al., 2018).

Therefore, this work allows stating that the pharmacological administration of low doses of melatonin during 21 days to lambs gestated and born under hypobaric hypoxia; has no significant effects on the passive mechanical behavior of the aorta and main pulmonary arteries. Furthermore, the microstructural changes seen are in agreement with recent research related to melatonin administration as an adjuvant in PHN cases. (Herrera et al., 2014a; Torres et al., 2015; Astorga et al., 2018; González-Candia, 2020).

Finally, this original research allowed reporting a set of experimental measurements of the mechanical behavior of arteries from animals exposed to high altitude (> 2500 masl), an hypoxic environment, with PHN.

Funding and acknowledgments

The work was funded by CONICYT-PCHA/Doctorado Nacional/2014–21140988 and projects FONDECYT 1170608 and 1151119.

We are grateful for the excellent technical assistance of Mr Gabino Llusco and Carlos Brito in animal maintenance and of Mrs. Mireya Delgado in the samples processing.

Author statement

All authors have made substantial contributions to all of the following:

E. Rivera: Conceptualization, Methodology, Validation, Formal analysis, Investigation, Writing - original draft, Writing - review & editing, Visualization. **C. García-Herrera**: Conceptualization, Methodology, Formal analysis, Investigation, Resources, Writing - original draft, Writing - review & editing, Supervision, Project administration, Funding acquisition. **A. González-Candia**: Methodology, Validation, Investigation, Writing - original draft, Writing - review & editing, Visualization. **D. Celentano**: Formal analysis, Investigation, Writing - original draft, Writing - review & editing. **E. Herrera**: Conceptualization, Methodology, Formal analysis, Investigation, Resources, Writing - original draft, Writing - review & editing, Supervision, Funding acquisition.

Declaration of competing interest

The authors declare that they have no known competing financial interests or personal relationships that could have appeared to influence the work reported in this paper.

References

Akentjew, Tamara L., et al., 2019. Rapid fabrication of reinforced and cell-laden vascular grafts structurally inspired by human coronary arteries. Nat. Commun. 3098 https://doi.org/10.1038/s41467-019-11090-3.

Arroyave, A.I., et al., 2015. Methodology for mechanical characterization of soft bio logical tissues: arteries. Procedia Eng. 110, 74–81. https://doi.org/10.1016/j._proeng.2015.07.012.

Astorga, Cristian R., et al., 2018. Melatonin decreases pulmonary vascular remodeling and oxygen sensitivity in pulmonary hypertensive newborn lambs. Front. Physiol. 9 (185), 1–11. https://doi.org/10.3389/fphys.2018.00185.

Aversa, Salvatore, et al., 2012. Potential utility of melatonin as an antioxidant during pregnancy and in the perinatal period. Front. Physiol. 25 (3), 207–221. https://doi.org/10.3109/14767058.2011.573827.

Baker, Jacquie, Kurt, Kimpinski, 2018. Role of melatonin in blood pressure regulation: an adjunct anti-hypertensive agent. Clin. Exp. Pharmacol. Physiol. 45 (8), 755–766. https://doi.org/10.1111/bcpt.13051.

Cabrera, M.S., et al., 2013. Mechanical analysis of ovine and pediatric pulmonary artery for heart valve stent design. J. Biomech. 46 (12), 2075–2081. https://doi.org/10.1016/j.jbiomech.2013.04.020.

Cañas, Daniel, et al., 2017. Fetal growth restriction induces heterogeneous effects on vascular biomechanical and functional properties in Guinea pigs (Cavia porcellus). Front. Physiol. 8, 1–9. https://doi.org/10.3389/fphys.2017.00144.

Carson, Freida, Hladik, Christa, 2009. *Histotechnology:* A Self-Instructional. 3rd. American Society for Clinical Pathology, ISBN 978-0891895817, p. 400.

Claes, Els, 2010. Mechanical study of human coronary arteries and their vascular grafts. [Ph.D.thesis] [in Spanish]. Tesis doctoral. Universidad Politécnica de Madrid, p. 304, 1. http://oa.upm.es/3859/.

Dan-Chen, Wu, et al., 2013. Pediatric pulmonary arterial hypertension. Curr. Hypertens. Rep. 15 (6), 606–613. https://doi.org/10.1007/s11906-013-0399-3.

Dodson, R. Blair, et al., 2013. Increased stiffness and extracellular matrix reorganization in intrauterine growth restricted (IUGR) fetal sheep. Pediatr. Res. 73, 147–154. https://doi.org/10.1038/pr.2012.156.

Dodson, R. Blair, et al., 2014. Thoracic and abdominal aortas stiffen through unique extracellular matrix changes in intrauterine growth restricted fetal sheep. Am. J. Physiol. Heart Circ. Physiol. 306, H429–H437. https://doi.org/10.1152/ajpheart.00472.2013.

Dong, Feng, et al., 2005. Maternal nutrient restriction during early to mid gestation up regulates cardiac insulin-like growth factor (IGF) receptors associated with enlarged ventricular size in fetal sheep. Growth Hormone IGF Res. 15 (4) https://doi.org/10.1016/j.ghir.2005.05.003, 291–466 299.

Dong, Feng, et al., 2008. Influence of maternal undernutrition and overfeeding on cardiac ciliary neurotrophic factor receptor and ventricular size in fetal sheep. J. Nutr. Biochem. 19 (6), 409–414. https://doi.org/10.1016/j.jnutbio.2007.06.003.

Drude, Fugelseth, et al., 2000. Ductus venosus flow velocity in newborn lambs during increased pulmonary artery pressure. Pediatr. Res. 47, 767–772. https://doi.org/10.1203/00006450-200006000-00014.

Eisele, John H., et al., 1986. Pulmonary vascular responses to nitrous oxide in newborn lambs. Anesth. Analg. 65, 62–64. https://doi.org/10.1203/00006450-200006000-00014.

Frid, Maria G., et al., 1994. Multiple phenotypically distinct smooth muscle cell populations exist in the adult and developing bovine pulmonary arterial media in vivo. Circ. Res. 75 (4), 669–681. https://doi.org/10.1161/01.res.75.4.669.

Fung, Yuan Cheng, 1991. What are the residual stresses doing in our blood vessels? Ann. Biomed. Eng. 19, 237–249. https://doi.org/10.1007/BF02584301.
Gao, Yuansheng, Raj, J Usha, 2011. THypoxic pulmonary hypertension of the new born. Compreh. Physiol. 1 (1), 61–79. https://doi.org/10.1002/cphy.c090015.
García-Herrera, Claudio, 2008. Mechanical behaviour of the human ascending aorta: characterization and numerical simulation [PhD thesis]. [in Spanish]: Universidad Politécnica de Madrid, p. 230, 1. http://oa.upm.es/1241/.
García-Herrera, Claudio, et al., 2012. Mechanical behaviour and rupture of normal and pathological human ascending aortic wall. Med. Biol. Eng. 50 (6), 559–566. https://doi.org/10.1007/s11517-012-0876-x.
García-Herrera, Claudio, et al., 2016. Mechanical analysis of the ring opening test applied to human ascending aortas. Comput. Methods Biomech. Biomed. Eng. 19 (16), 1738–1748. https://doi.org/10.1080/10255842.2016.1183125.
Gasque, Juan, 2009. Persistent pulmonary hypertension of the newborn (in spanish). Rev. Mex. Pediatría 76 (5), 220–230.
GIMP-team, 2014. GIMP plugin registry. In: A Repository of Optional Extensions for the GIMP [date unknown], [Internet]. https://www.gimp.org/.
González-Candia, A., et al., 2016. Potential adverse effects of antenatal melatonin as a treatment for intrauterine growth restriction: findings in pregnant sheep. Am. J. Obstet. Gynecol. 215 (2) https://doi.org/10.1016/j.ajog.2016.02.040. P245.e1–245.e7.
González-Candia, A., et al., 2020. Melatonin long-lasting beneficial effects on pulmonary vascular reactivity and redox balance in chronic hypoxic ovine neonates. J. Pineal Res. 68 (1) https://doi.org/10.1111/jpi.12613 e12613.
Greenwald, S.E., et al., 1997. Experimental investigation of the distribution of residual strains in the artery wall. J. Biomech. Eng. 119 (4), 438–444. https://doi.org/10.1115/1.2798291.
Hanson, M.A., Gluckman, P.D., 2014. Early developmental conditioning of later Health and disease: physiology or pathophysiology? Physiol. Rev. 94 (4) https://doi.org/10.1152/physrev.00029.2013.
Hanson, Mark, 2019. The inheritance of cardiovascular disease risk. Acta Peadiatr. 108 (10), 1747–1756. https://doi.org/10.1111/apa.14813.
Herrera, E.A., et al., 2008. Sildenafil reverses hypoxic pulmonary hypertension in highland and lowland newborn sheep. Pediatr. Res. 63, 169–175. https://doi.org/10.1203/PDR.0b013e31815ef71c.
Herrera, E.A., et al., 2015. Pharmacological approaches in either intermittent or permanent hypoxia: a tale of two exposures. Pharmacol. Res. 101, 94–101. https://doi.org/10.1016/j.phrs.2015.07.011.
Hernández-Díaz, S., et al., 2007. Risk factors for persistent pulmonary hypertension of the newborn. Pediatrics 120 (2), e272–e282. https://doi.org/10.1542/peds.2006-3037.
Herrera, Emilio A., et al., 2007. High-altitude chronic hypoxia during gestation and after birth modifies cardiovascular responses in newborn sheep. Am. J. Physiol. Regul. Integr. Comp. Physiol. 292 (6), 2234–2240. https://doi.org/10.1152/ajpregu.00909.2006.
Herrera, Emilio A., et al., 2014a. Melatonin improves cerebrovascular function and de creases oxidative stress in chronically hypoxic lambs. J. Pineal Res. 57 (1), 33–42. https://doi.org/10.1111/jpi.12141.
Herrera, Emilio A., et al., 2014b. The placental pursuit for an adequate oxidant balance between the mother and the fetus. Front. Pharmacol. 149, 5. https://doi.org/10.3389/fphar.2014.00149.
Holzapfel, Gerhard A., 2006. Determination of material models for arterial walls from uniaxial extension tests and histological structure. J. Theor. Biol. 238, 290–302. https://doi.org/10.1016/j.jtbi.2005.05.006.
Holzapfel, Gerhard A., et al., 2007. Layer-specific 3D residual deformations of hu man aortas with non-atherosclerotic intimal thickening. Ann. Biomed. Eng. 35 (4), 530–545. https://doi.org/10.1007/s10439-006-9252-z.
Horny, Lukas, et al., 2013. Analysis of axial pre-stretch in the abdominal aorta with reference to post mortem interval and degree of atherosclerosis. J. Mech. Behav. Biomed. Mater. 33, 93–98. https://doi.org/10.1016/j.jmbbm.2013.01.033.
Horny, Lukas, et al., 2014. Axial prestretch and circumferential distensibility in biomechanics of abdominal aorta. Biomech. Model. Mechanobiol. 13, 783–799. https://doi.org/10.1007/s10237-013-0534-8.
Jain, Amish, McNamara, Patrick J., 2015. THypoxic pulmonary hypertension of the newborn. Semin. Fetal Neonatal Med. 20 (4), 262–271. https://doi.org/10.1016/j.siny.2015.03.001.
Kandadi, Machender R., et al., 2013. Influence of gestational overfeeding on myocardial pro-inflammatory mediators in fetal sheep heart. J. Nutr. Biochem. 19 (6), 1982–1990. https://doi.org/10.1016/j.jnutbio.2013.07.003.
Kassab, Ghassan S., 2006. Biomechanics of the cardiovascular system:the aorta as an illustratory example. J. R. Soc. Interface 3, 719–740. https://doi.org/10.1098/rsif.2006.0138.
Keyes, L.E., et al., 2003. Intrauterine growth restriction, preeclampsia, and intrauterine mortality at high altitude in Bolivia. Pediatr. Res. 54, 20–25. https://doi.org/10.1203/01.PDR.0000069846.64389. DC.
Laurent, S., et al., 2006. Expert consensus document on arterial stiffness: methodological issues and clinical applications. Eur. Heart J. 27, 2588–2605. https://doi.org/10.1093/eurheartj/ehl254.
Liu, S.Q., Fung, Y.C., 1988. Zero-stress states of arteries. J. Biomech. Eng. 110 (1), 82–84. https://doi.org/10.1115/1.3108410.
Macrae, R.A., et al., 2016. Methods in mechanical testing of arterial tissue: a review. Strain 52 (5), 380–399. https://doi.org/10.1111/str.12183.
Meyrick, B., Reid, L., 1982. Normal postnatal development of the media of rat hiliar pulmonary artery and its remodelling by chronic hypoxia. Lab. Invest. 46 (5), 505–514.
Okamoto, R.J., et al., 2002. Mechanical properties of dilated human ascending aorta. Ann. Biomed. Eng. 30 (5), 624–635. https://doi.org/10.1114/1.1484220.
Papamatheakis, D.G., et al., 2013. Antenatal hypoxia and pulmonary vascular function and remodeling. Curr. Vasc. Pharmacol. 11 (5), 616–640. https://doi.org/10.2174/1570161111311050006.
Pedersen, Jonas, et al., 2018. Current and future treatments for persistent pulmonary hypertension in the newborn. Semin. Fetal Neonatal Med. 123 (4), 392–406. https://doi.org/10.1111/bcpt.13051.
Peers, A., et al., 2002. Blood pressure, heart rate, hormonal and other acute responses to rubber-ring castration and tail docking of lambs. N. Z. Vet. J. 2 (50), 56–62. https://doi.org/10.1080/00480169.2002.36251.
Rood, Kristiana, et al., 2019. Gestational hypoxia and programming of lung metabolism. Front. Physiol. 10, 1453. https://doi.org/10.3389/fphys.2019.01453.
Schepelmann, Martin, et al., 2011. The presence and localization of melatonin receptors in the rat aorta. Cell. Mol. Neurobiol. 31 (8), 1257–1265. https://doi.org/10.1007/s10571-011-9727-9.
Schneider, C.A., et al., 2012. NIH Image to ImageJ: 25 years of image analysis. Nat. Methods 9 (7), 671–675. https://doi.org/10.1038/nmeth._2089.
Stenmark, K.R., et al., 1987. Severe pulmonary hypertension and arterial adventitial changes in newborn calves at 4,300 m. J. Appl. Physiol. 62 (2), 821–830. https://doi.org/10.1152/jappl.1987.62.2.821.
Sun, Hang, et al., 2016. Effects of melatonin on cardiovas cular diseases: progress in the past year. Curr. Opin. Lipidol. 27 (4), 408–413. https://doi.org/10.1097/mol.0000000000000314.
Thelitz, Stephan, et al., 2004. Inhaled nitric oxide decreases pulmonary solubleguanylate cyclase protein levels in 1-month-old lambs. J. Thorac. Cardiovasc. Surg. 127 (5), 1285–1292. https://doi.org/10.1016/j.jtcvs.2003.07.024.
Torres, Flavio, et al., 2015. Melatonin reduces oxidative stress and improves vascular function in pulmonary hypertensive newborn sheep. J. Pineal Res. 58 (3), 362–373. https://doi.org/10.1111/jpi.12222.
Vaishnav, Ramesh N., Vossoughi, Jafar, 1983. Estimation of residual strains in aortic segments. In: Proceedings of the Second Southern Biomedical Engineering Conference, pp. 330–333. https://doi.org/10.1016/B978-0-08-030145-7.50078-7.
Wells, S.M., et al., 1999. Determinants of mechanical properties in the developing ovine thoracic aorta. Am. J. Physiol. Heart Circ. Physiol. 277 (4), H1385–H1391. https://doi.org/10.1152/ajpheart.1999.277.4.H1385.
Zhou, Hao, et al., 2018. Protective role of melatonin in cardiac ischemia-reperfusion injury: from pathogenesis to targeted therapy. J. Pineal Res. 64 (3), 1–21. https://doi.org/10.1111/jpi.12471.